A new family of finite elements for wrinkling analysis of thin films on compliant substrates

Jie Yang, Qun Huang, Heng Hu, Gaetano Giunta, Salim Belouettar, Michel Potier-Ferry

A new family of finite elements for wrinkling analysis of thin films on compliant substrates

Jie Yang [a], Qun Huang [a], Heng Hu [a,*], Gaetano Giunta [b], Salim Belouettar [b], Michel Potier-Ferry [c,d]

[a] School of Civil Engineering, Wuhan University, 8 South Road of East Lake, Wuchang, 430072 Wuhan, PR China
[b] Centre de Recherche Public Henri Tudor, 29, av. John F. Kennedy, L-1855 Luxembourg-Kirchberg, Luxembourg
[c] Laboratoire d'Etude des Microstructures et de Mécanique des Matériaux, LEM3, UMR CNRS 7239, Université de Lorraine, Ile du Saulcy, 57045 Metz Cedex 01, France
[d] Laboratory of Excellence on Design of Alloy Metals for low-mAss Structures (DAMAS), Université de Lorraine, France

This paper presents a new one-dimensional finite elements' family for the analysis of wrinkling in stiff thin films resting on a thick elastic substrate. Euler–Bernoulli's theory is used for the thin film, whereas the substrate is ideally divided into two parts: 1. a core layer in the neighbourhood of the film where the displacement field presents high gradients (where an higher-order approximation is required) and 2. the remaining part of the substrate or bottom layer where displacements change very slowly. Low-order models allow an accurate yet efficient description of this latter part. Due to its versatility and generality, Carrera's Unified Formulation is used to develop the proposed elements' family. Governing equations' weak form is derived by means of the principle of virtual displacements and discretised in a finite ele-ment sense. The asymptotic numerical method is used to solve the resulting non-linear equations' sys-tem. Numerical investigations show that the proposed one-dimensional elements are able to capture the instability phenomena in film-substrate systems. In order to validate the proposed finite element models, the critical loads and half-wave numbers predicted by the one-dimensional elements are com-pared with those obtained via two-dimensional finite element analyses and a very good agreement is found.

1. Introduction

Wrinkling instabilities of different shapes (stripes, labyrinths, or herringbones) are very common in several structural configurations. In particular, they very likely to occur in thin stiff films or coatings resting on compliant substrates and subjected to in-plane mechanical or thermal loads, see Bowden et al. [1]. These systems find several applications in several engineering fields spanning from optics and electronics to aeronautics and space as, for instance, optical and acoustic devices or skin layers in sandwich composites. Furthermore, the interest on soft polymeric substrates is more and more increasing, see Volynskii et al. [2] and Cao and Hutchinson [3]. For these reasons, an accurate yet effective modelling of wrinkling instabilities is a very important and up-to-date research topic.

A brief literature follows. In the framework of sandwich panels design, Allen [4] investigated wrinkles in very stiff thin films when compared to the substrate they resting on. Niu and Talreja [5] determined the critical membrane force and the wrinkles wavelength in sandwich panels on the basis of a linear perturbation analysis. A unified analytical expression for single-sided face, in-phase and out-of-phase wrinkling was presented. Huang et al. [6] proposed a spectral method for modelling wrinkles' evolution where a Winkler foundation (a foundation made of linear springs) was accounted for. The model was extended to the case of a thick elastic foundation in Huang et al. [7] where wavelength and amplitude for various moduli and thicknesses of the substrate in the case of wrinkles (a pattern that is invariant in one direction) were investigated. Audoly and Boudaoud [8–10] studied the straight and herringbones wrinkles as well as the evolution form the former type (due to a moderate load) to the latter one (large buckling) as the external load is increased. Wang et al. [11] investigated both global and local buckling in thin films and membranes resting on elastomeric substrates. An analytical expression for the critical condition separating these two buckling modes was presented and compared with experimental and numerical results. The post-buckling evolution of surface wrinkles was studied by Zang et al. [12] by numerical (finite elements) and analytical models. Several higher-order wrinkling modes were observed. Experiments were also carried

* Corresponding author.
E-mail address: huheng@whu.edu.cn (H. Hu).

out. Stemming form the work by Damil and Potier-Ferry [13], Hu et al. [14] and Xu et al. [15] studied the global and local buckling of long beams resting on a non-linear elastic foundation by means of a multi-scale approach. A Fourier series approximation with slowly varying coefficients was coupled to a refined model by means of the Arlequin method. In such a manner, accurate solutions were obtained at the structural boundaries where the approximated approaches are known to provide poor results.

In this paper, a family of one-dimensional finite elements for the analysis of sinusoidal wrinkling in stiff films resting on thick elastic substrates is presented. A variable through-the-thickness kinematics is implemented by means of Carrera's Unified Formulation (CUF), see Carrera [16], Carrera and Giunta [17–19], Catapano et al. [20] and He et al. [21]. The main aim is to exploit the features of the problem under investigation to propose a family of finite elements that yields accurate results with a number of degrees of freedom as reduced as possible. In particular, the thin film is modelled via Euler–Bernoulli's kinematics. The substrate is ideally divided into two parts where a variable kinematics based upon Taylor's polynomial series expansion is used. The displacement fields expansion order is not a priori fixed but it is a free parameter. The idea of subdividing the substrate aims at effectively and efficiently modelling the substrate mechanical behaviour that plays a very important role in the formation of instability patterns. In a limited neighbourhood of the thin film within the substrate, the displacement field presents a very high through-the-thickness gradient. On the contrary, the remaining part of the substrate is almost unstrained. It is, then, clear that for the former part, called "boundary or core layer", a higher-order kinematics is necessary, whereas a low-order kinematics is sufficient for the substrate "bottom layer". The governing equations are obtained by the virtual work principle and their discrete form is obtained within the framework of the finite element method. The Asymptotic Numerical Method (ANM) is used to solve the non-linear problem, see Damil and Potier-Ferry [22], Cochelin et al. [23,24], Hu et al. [25] and Liu et al. [26]. ANM offers several advantages in terms of computation time and reliability when compared to classical non-linear solution strategies such as Newton–Raphson's and arc-length methods. Analysis investigates the critical wrinkling loads and pattern (in terms of the half-waves number). The effectiveness of different kinematics is studied. Some parametric analyses are carried out to obtain some indications on the appropriate thickness of the core layer. This latter has been related to the wrinkles' wavelength. The proposed elements are assessed towards numerical simulations performed by the commercial finite element software ABAQUS using two-dimensional elements. Very accurate results are obtained and the computational effort is considerably reduced.

2. Model kinematics

A two-dimensional elastic stiff film bound to an elastic soft compliant substrate is considered, see Fig. 1. Skin's and substrate's thickness are addressed by h_f and h_s, whereas h is the total thickness. The substrate is ideally divided into a core and a bottom layer of thickness h_c and h_b. This division allows to describe the rapid variation of the displacement field in the neighbourhood of the thin film by means of high-order kinematic theories, whereas low-order polynomials are used to model the slowly varying kinematics far away from the top membrane. The length and the width of the structure are denoted by L and b. The longitudinal, the through-the-width and the transverse coordinate are x, y and z.

The displacement field is:

$$\mathbf{u}^T(x,z) = \{u(x,z), w(x,z)\} \tag{1}$$

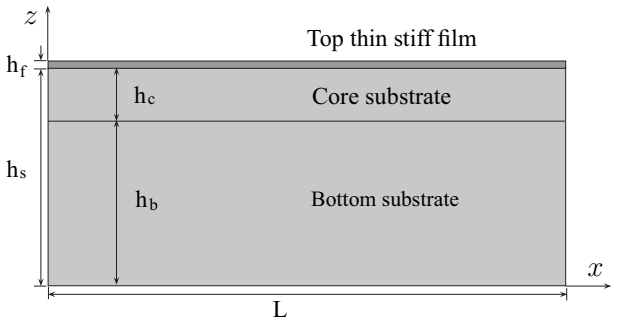

Fig. 1. An elastic thin stiff film on a thick elastic compliant substrate ideally divided into core and bottom layers.

where u and w are the components along x- and z-axis, respectively. T as superscript stands for the transposition operator. According to a one-dimensional modelling approach, the variation along the through-the-thickness direction of the displacement field is a priori assumed. Classically, a polynomial variation of a fixed order n is considered. Within CUF framework, a family of refined beam models can be systematically obtained considering the polynomial approximation order as a free parameter of the formulation, that is, it can assume an arbitrary value. The displacement field in Eq. (1) is approximated as a linear combination of the following monomial terms:

$$\mathbf{u}(x,z) = F_\tau(z)\mathbf{u}_\tau(x) \qquad \tau \in [0,n] \subset \mathbb{N} \tag{2}$$

F_τ represents the through-the-thickness approximating function and, in general, it can be an element of a generic approximation base. Within this work, Mac Laurin's polynomials z^n are adopted as approximation or expansion function. Function $\mathbf{u}_\tau$ accounts for the variation along the beam axis. This latter term depends upon the method used to solve the governing equation. Einstein's compact notation has been used in Eq. (2): a repeated index implicitly implies summation over its variation range:

$$\begin{aligned} u &= u_0 + zu_1 + z^2u_2 + \cdots + z^nu_n \\ w &= w_0 + zw_1 + z^2w_2 + \cdots + z^nw_n \end{aligned} \tag{3}$$

A different kinematic model is independently defined for the thin-film and the substrate core and bottom layers:

$$\mathbf{u}(x,z): \begin{cases} u^f(x,z) = u^f_0(x) - \left(z - \frac{h_f+2h_s}{2}\right) w^f_{0,x}(x) \\ w^f(x,z) = w^f_0(x) \end{cases} \quad z \in \left[h_s, h_s+h_f\right] \tag{4}$$

$$\mathbf{u}(x,z): \begin{cases} u^c(x,z) = F_\tau u^c_\tau(x) \\ w^c(x,z) = F_\tau w^c_\tau(x) \end{cases} \quad z \in [h_b, h_s] \ \tau \in [0,n_c] \tag{5}$$

$$\mathbf{u}(x,z): \begin{cases} u^b(x,z) = F_\tau u^b_\tau(x) \\ w^b(x,z) = F_\tau w^b_\tau(x) \end{cases} \quad z \in [0,h_b] \ \tau \in [0,n_b] \tag{6}$$

where superscripts f, c and b stands for film, core and bottom, respectively. Euler–Bernoulli kinematics' is used to model the top film. Through-the-thickness shear and normal deformations are, therefore, disregarded there. This assumption is justified by the thinness of the film. Subscript x preceded by comma stands for differentiation versus the axial coordinate. A CUF variable order kinematics is used for the substrate core and bottom layers where the expansion order is n_c and n_b, respectively.

The continuity of the displacements along the thickness direction is ensured by the following congruency equations:

$$\begin{aligned} &u^f(x,h_s) = u^c(x,h_s) \\ &w^f(x,h_s) = w^c(x,h_s) \\ &u^c(x,h_b) = u^b(x,h_b) \\ &w^c(x,h_b) = w^b(x,h_b) \end{aligned} \quad \forall x \in [0,L] \tag{7}$$

By replacing Eqs. (4) and (5) into Eq. (7), the displacements continuity at the interface between the film and the substrate core layer results in the following relations:

$$\begin{aligned} u_0^c &= u_0^f + \tfrac{1}{2} h_f w_{0,x}^f - \overline{F}_i u_i^c \\ w_0^c &= w_0^f - \overline{F}_i w_i^c \end{aligned} \qquad i \in [1, n_c] \tag{8}$$

where $\overline{F}_i = h_s^i$ and Eq. (5) read:

$$\begin{aligned} u^c &= u_0^f + \tfrac{h_f}{2} w_{0,x}^f + (F_i - \overline{F}_i) u_i^c \\ w^c &= w_0^f + (F_i - \overline{F}_i) w_i^c \end{aligned} \qquad z \in [h_b, h_s]\ i \in [1, n_c] \tag{9}$$

The congruency of the displacements at interface $\Gamma = \{(x,y,z) : x \in [0,L], y \in [-b/2, +b/2], z = h_b\}$ between core and bottom layers is enforced by accounting for Eqs. (7)c and (7)d through the Lagrange multiplier $\boldsymbol{\mu}^T = \{\mu_1, \mu_2\}$. This results in the constrain term $\mathscr{C}(\boldsymbol{\mu}, \mathbf{u})$:

$$\mathscr{C}(\boldsymbol{\mu}, \mathbf{u}) = \int_\Gamma \{\mu_1 [u^c(x,h_b) - u^b(x,h_b)] + \mu_2 [w^c(x,h_b) - w^b(x,h_b)]\} d\Gamma \tag{10}$$

This term is considered within the principle of virtual displacement when deriving the weak form of the problem governing equations.

3. Governing equations

3.1. Geometric equations and constitutive law

A non-linear geometric equation in a Von Karman sense is considered for the thin film:

$$\varepsilon_{xx}^f = u_{,x}^f + \frac{1}{2}\left(w_{,x}^f\right)^2 \tag{11}$$

whereas the substrate is considered to undergo small displacements and rotations:

$$\begin{aligned} \varepsilon_{xx}^s &= u_{,x}^s \\ \varepsilon_{zz}^s &= w_{,z}^s \\ \gamma_{xz}^s &= u_{,z}^s + w_{,x}^s \end{aligned} \tag{12}$$

Superscript s in Eq. (12) generically indicates a substrate layer (either the core or the bottom one).

As far as the material constitutive behaviour is concerned, Hooke's law is assumed. The material is, therefore, linear and elastic. Furthermore, isotropic films and substrates are considered. The displacement field in Eqs. (4)–(6) results in the plane strain condition:

$$\varepsilon_{yy} = \varepsilon_{xy} = \varepsilon_{yz} = 0 \tag{13}$$

The following full three-dimensional Hooke's law is, then, used for the substrate:

$$\begin{aligned} \sigma_{xx}^s &= C_{11}^s \varepsilon_{xx}^s + C_{13}^s \varepsilon_{zz}^s \\ \sigma_{zz}^s &= C_{13}^s \varepsilon_{xx}^s + C_{33}^s \varepsilon_{zz}^s \\ \sigma_{xz}^s &= C_{55}^s \varepsilon_{xz}^s \end{aligned} \tag{14}$$

with:

$$\begin{aligned} C_{11}^s = C_{33}^s &= \frac{1 - \nu^s}{(1+\nu^s)(1-2\nu^s)} E^s \\ C_{13}^s &= \frac{\nu^s}{(1+\nu^s)(1-2\nu^s)} E^s \\ C_{55}^s &= \frac{E^s}{2(1+\nu^s)} \end{aligned} \tag{15}$$

where E^s and ν^s are the substrate material Young modulus and Poisson ratio. A reduced form of Hooke's law has to be assumed for the thin film since Euler–Bernoulli's kinematics accounts for the strain components ε_{xx}^f only. This clearly violates the strain coupling:

$$\varepsilon_{yy}^f = \varepsilon_{zz}^f = -\nu^f \varepsilon_{xx}^f \neq 0 \tag{16}$$

due to Poisson's ratio. This phenomenon is commonly known in literature as Poisson locking, see Carrera and Brischetto [27]. In the case of one-dimensional modelling, Hooke's law should be corrected as outlined in Giunta et al. [28], resulting in the following constitutive equation:

$$\sigma_{xx}^f = E^f \varepsilon_{xx}^f \tag{17}$$

where E^f is the Young modulus of the film.

3.2. Virtual work equation

The weak form of the governing equations are obtained by means of a constrained variational problem through the Principle of Virtual Displacement where the displacement congruency on Γ is enforced by means of a Lagrange multiplier:

$$\delta \mathscr{L}_{int} + \delta \mathscr{C} = \delta \mathscr{L}_{ext} \tag{18}$$

where δ stands for a virtual variation, $\mathscr{L}_{int}$ is the internal work, $\mathscr{L}_{ext}$ the work done by external forces and $\mathscr{C}$ has been defined in Eqs. (10).

3.2.1. Internal virtual work

The internal virtual work is expressed as:

$$\delta \mathscr{L}_{int} = \delta \mathscr{L}_{int}^f + \delta \mathscr{L}_{int}^c + \delta \mathscr{L}_{int}^b \tag{19}$$

The virtual internal work of the film is:

$$\delta \mathscr{L}_{int}^f = \int_{V^f} \delta \varepsilon_{xx}^f \sigma_{xx}^f dV \tag{20}$$

where V^f is the volume of the film (V^c and V^b are those of the core and bottom substrate layers). After replacing Eqs. (17) and (11) and integrating over the thin film cross-section, Eq. (20) reads:

$$\delta \mathscr{L}_{int}^f = \int_L \left[N^f \left(\delta u_{0,x}^f + w_{0,x}^f \delta w_{0,x}^f \right) - M^f \delta w_{0,xx}^f \right] dx \tag{21}$$

where N^f and M^f are the resulting axial force and bending moment:

$$\begin{aligned} N^f &= \int_{h_s}^{h_s+h_f} \int_{-\frac{b}{2}}^{+\frac{b}{2}} \sigma_{xx}^f \, dy \, dz = b h_f E^f \left(u_{0,x}^f + \frac{1}{2} w_{0,x}^{f2} \right) \\ M^f &= \int_{h_s}^{h_s+h_f} \int_{-\frac{b}{2}}^{+\frac{b}{2}} \left(z - \frac{h_f + 2h_s}{2} \right) \sigma_{xx}^f \, dy \, dz = -\frac{b h_f^3}{12} E^f w_{0,xx}^f \end{aligned} \tag{22}$$

Eq. (21) can be written in the following matrix form:

$$\delta \mathscr{L}_{int}^f = \int_L \delta \mathbf{v}_f^T \left[\mathbf{H}^T + \mathbf{A}^{fT}(\mathbf{v}_f) \right] \mathbf{S}^f dx \tag{23}$$

where:

$$\mathbf{v}_f^T = \{ u_{0,x} \quad w_{0,x} \quad w_{0,xx} \} \tag{24}$$

$$\mathbf{H} = \begin{bmatrix} 1 & 0 & 0 \\ 0 & 0 & -1 \end{bmatrix} \tag{25}$$

$$\mathbf{A}^f(\mathbf{v}_f) = \begin{bmatrix} 0 & w_{0,x}^f & 0 \\ 0 & 0 & 0 \end{bmatrix} \tag{26}$$

and:

$$\mathbf{S}^f = \{ N^f \quad M^f \}^T \tag{27}$$

The film resultant vector $\mathbf{S}^{fT}$ in Eq. (27) can be rewritten in terms of displacements by considering Eq. (22):

$$\mathbf{S}^f = \mathbf{D}^f \left[\mathbf{H} + \frac{1}{2} \mathbf{A}^f (\mathbf{v}_f) \right] \mathbf{v}_f \tag{28}$$

where $\mathbf{D}^f$ being a diagonal matrix accounting for the membrane and bending stiffness term typical of the Euler–Bernoulli kinematics:

$$\mathbf{D}^f = E^f \begin{bmatrix} bh_f & 0 \\ 0 & \frac{1}{12} bh_f^3 \end{bmatrix} \tag{29}$$

As far as the substrate is concerned, its internal virtual work is the sum of two contributes since it has been ideally divided into core and bottom layers:

$$\delta \mathscr{L}^s_{int} = \delta \mathscr{L}^c_{int} + \delta \mathscr{L}^b_{int} \tag{30}$$

$\delta \mathscr{L}^c_{int}$ is defined as:

$$\delta \mathscr{L}^c_{int} = \int_{V^c} \left(\delta \varepsilon^c_{xx} \sigma^c_{xx} + \delta \varepsilon^c_{zz} \sigma^c_{zz} + \delta \gamma^c_{xz} \sigma^c_{xz} \right) dV \tag{31}$$

After replacing the geometric relations in Eq. (12), the displacement field approximation in Eq. (9) and by integrating over the beam cross section, Eq. (31) reads:

$$\begin{aligned} \delta \mathscr{L}^c_{int} = \int_L \Big(& N^c_{xx0} \delta u^f_{0,x} + M^c_{xx0} \delta w^f_{0,xx} + T^c_{xz0} \delta w^f_{0,x} + M^c_{xxi} \delta u^c_{i,x} + M^c_{xzui} \delta u^c_i \\ & + M^c_{zzi} \delta w^c_i + M^c_{xzwi} \delta w^c_{i,x} \Big) dx \end{aligned} \tag{32}$$

The core stress resultants are:

$$\begin{aligned} \frac{N^c_{xx0}}{b} &= \int_{h_b}^{h_s} \sigma^c_{xx} dz = J^{11c}_{00} \left(u^f_{0,x} + \frac{h_f}{2} w^f_{0,xx} \right) + J^{11c}_{0j} u^c_{j,x} + J^{13c}_{0j,z} w^c_j \\ \frac{M^c_{xx0}}{b} &= \frac{h_f}{2} \int_{h_b}^{h_s} \sigma^c_{xx} dz = \frac{h_f}{2} \frac{N^c_{xx0}}{b} \\ \frac{T^c_{xz0}}{b} &= \int_{h_b}^{h_s} \sigma^c_{xz} dz = J^{55c}_{00} w^f_{0,x} + J^{55c}_{0j,z} u^c_j + J^{55c}_{0j} w^c_{j,x} \\ \frac{M^c_{xxi}}{b} &= \int_{h_b}^{h_s} \sigma^c_{xx} (F_i - \overline{F}_i) dz = J^{11c}_{i0} \left(u^f_{0,x} + \frac{h_f}{2} w^f_{0,xx} \right) + J^{11c}_{ij} u^c_{j,x} + J^{13c}_{ij,z} w^c_j \\ \frac{M^c_{xzwi}}{b} &= \int_{h_b}^{h_s} \sigma^c_{xz} (F_i - \overline{F}_i) dz = J^{55c}_{i0} w^f_{0,x} + J^{55c}_{ij,z} u^c_j + J^{55c}_{ij} w^c_{j,x} \\ \frac{M^c_{zzi}}{b} &= \int_{h_b}^{h_s} \sigma^c_{zz} F_{i,z} dz = J^{13c}_{i,z0} \left(u^f_{0,x} + \frac{h_f}{2} w^f_{0,xx} \right) + J^{13c}_{i,zj} u^c_{j,x} + J^{33c}_{i,zj,z} w^c_j \\ \frac{M^c_{xzui}}{b} &= \int_{h_b}^{h_s} \sigma^c_{xz} F_{i,z} dz = J^{55c}_{i,z0} w^f_{0,x} + J^{55c}_{i,zj,z} u^c_j + J^{55c}_{i,zj} w^c_{j,x} \end{aligned} \tag{33}$$

where:

$$\begin{aligned} J^{mnc}_{00} &= \int_{h_b}^{h_s} C^c_{mn} dz = C^c_{mn} h_c \\ J^{mnc}_{ij} &= \int_{h_b}^{h_s} C^c_{mn} (F_i - \overline{F}_i)(F_j - \overline{F}_j) dz \\ &= C^c_{mn} \Bigg\{ \frac{ij(i+j+2)}{(i+1)(j+1)(i+j+1)} h_s^{i+j+1} \\ &\quad - h_b \left[h_s^i \quad h_s^j - \frac{h_b^j}{j+1} \right) + h_b^i \quad \frac{h_b^j}{i+j+1} - \frac{h_s^j}{i+1} \Bigg) \Bigg] \Bigg\} \\ J^{mnc}_{i,zj,z} &= \int_{h_b}^{h_s} C^c_{mn} F_{i,z} F_{j,z} dz = C^c_{mn} \frac{ij}{i+j+1} \left(h_s^{i+j+1} - h_b^{i+j+1} \right) \\ J^{mnc}_{0j} &= \int_{h_b}^{h_s} C^c_{mn} (F_j - \overline{F}_j) dz = C^c_{mn} \frac{1}{j+1} \left\{ h_b \left[(j+1) h_s^j - h_b^j \right] - j h_s^{j+1} \right\} \\ J^{mnc}_{i0} &= \int_{h_b}^{h_s} C^c_{mn} (F_i - \overline{F}_i) dz = C^c_{mn} \frac{1}{i+1} \left\{ h_b \left[(i+1) h_s^i - h_b^i \right] - i h_s^{i+1} \right\} \end{aligned}$$

$$\begin{aligned} J^{mnc}_{0j,z} &= \int_{h_b}^{h_s} C^c_{mn} F_{j,z} dz = h_s^j - h_b^j \\ J^{mnc}_{i,z0} &= \int_{h_b}^{h_s} C^c_{mn} F_{i,z} dz = h_s^i - h_b^i \\ J^{mnc}_{ij,z} &= \int_{h_b}^{h_s} C^c_{mn} (F_i - \overline{F}_i) F_{j,z} dz = C^c_{mn} \frac{1}{i+j} \left\{ h_b^j \left[(i+j) h_s^i - j h_b^i \right] - i h_s^{i+j} \right\} \\ J^{mnc}_{i,zj} &= \int_{h_b}^{h_s} C^c_{mn} (F_j - \overline{F}_j) F_{i,z} dz = C^c_{mn} \frac{1}{i+j} \left\{ h_b^i \left[(i+j) h_s^j - i h_b^j \right] - j h_s^{i+j} \right\} \end{aligned} \tag{34}$$

By accounting for Eqs. (33) and (32) can be rewritten in a compact matrix form in terms of displacements:

$$\delta \mathscr{L}^c_{int} = \int_L \delta \mathbf{v}_c^T \widetilde{\mathbf{K}}_c \mathbf{v}_c dx \tag{35}$$

where $\mathbf{v}_c \in \mathbb{R}^{4n_c+3}$ is vector whose components are the core generalised displacement unknown functions and their derivatives versus the axial coordinate. It is organised as follows:

$$\begin{aligned} \mathbf{v}_c^T = \Big\{ & u^f_{0,x} \quad w^f_{0,x} \quad w^f_{0,xx} \quad u^c_1 \quad \cdots \quad u^c_{n_c} \quad u^c_{1,x} \quad \cdots \quad u^c_{n_c,x} \quad w^c_1 \quad \cdots \\ & w^c_{n_c} \quad w^c_{1,x} \quad \cdots \quad w^c_{n_c,x} \Big\} \end{aligned} \tag{36}$$

$\widetilde{\mathbf{K}}_c \in \mathbb{R}^{(4n_c+3)\times(4n_c+3)}$ is the core layer stiffness matrix and it is not here explicitly reported for the sake of brevity. Its terms $\widetilde{K}_{ckl}$ are the coefficients of the products $\delta q_{ck} q_{cl}$ in Eqs. (32) and (33).

The internal virtual work of the bottom layer:

$$\delta \mathscr{L}^b_{int} = \int_{V^b} \left(\delta \varepsilon^b_{xx} \sigma^b_{xx} + \delta \varepsilon^b_{zz} \sigma^b_{zz} + \delta \gamma^b_{xz} \sigma^b_{xz} \right) dV \tag{37}$$

is treated in a manner similar to that of the core. After replacing Eq. (6) and integrating over through-the-thickness and -width coordinates, it reads:

$$\delta \mathscr{L}^b_{int} = \int_L \left(M^b_{xx\tau} \delta u^b_{\tau,x} + M^b_{zz\tau} \delta w^b_\tau + M^b_{xzu\tau} \delta u^b_\tau + M^b_{xzw\tau} \delta w^b_{\tau,x} \right) dx \tag{38}$$

The stress resultants in the bottom layer are:

$$\begin{aligned} \frac{M^b_{xx\tau}}{b} &= \int_0^{h_b} \sigma^b_{xx} F_\tau dz = J^{11b}_{\tau\sigma} u^b_{\sigma,x} + J^{13b}_{\tau\sigma,z} w^b_\sigma \\ \frac{M^c_{zz\tau}}{b} &= \int_0^{h_b} \sigma^b_{zz} F_{\tau,z} dz = J^{13b}_{\tau,z\sigma} u^b_{\sigma,x} + J^{33b}_{\tau,z\sigma,z} w^b_\sigma \\ \frac{M^c_{xzu\tau}}{b} &= \int_0^{h_b} \sigma^b_{xz} F_{\tau,z} dz = J^{55b}_{\tau,z\sigma,z} u^b_\sigma + J^{55b}_{\tau,z\sigma} w^b_{\sigma,x} \\ \frac{M^b_{xzw\tau}}{b} &= \int_0^{h_b} \sigma^b_{xz} F_\tau dz = J^{55b}_{\tau\sigma,z} u^b_\sigma + J^{55b}_{\tau\sigma} w^b_{\sigma,x} \end{aligned} \tag{39}$$

with:

$$\begin{aligned} J^{mnb}_{\tau\sigma} &= \int_0^{h_b} C^b_{mn} F_\tau F_\sigma dz = \frac{1}{\tau+\sigma+1} C^b_{mn} h_b^{\tau+\sigma+1} \\ J^{mnb}_{\tau,z\sigma,z} &= \int_0^{h_b} C^b_{mn} F_{\tau,z} F_{\sigma,z} dz = \frac{\tau\sigma}{\tau+\sigma-1} C^b_{mn} h_b^{\tau+\sigma-1} \\ J^{mnb}_{\tau,z\sigma} &= \int_0^{h_b} C^b_{mn} F_{\tau,z} F_\sigma dz = \frac{\tau}{\tau+\sigma} C^b_{mn} h_b^{\tau+\sigma} \\ J^{mnb}_{\tau\sigma,z} &= \int_0^{h_b} C^b_{mn} F_\tau F_{\sigma,z} dz = \frac{\sigma}{\tau+\sigma} C^b_{mn} h_b^{\tau+\sigma} \end{aligned} \tag{40}$$

The compact matrix form in terms of generalised displacements of Eqs. (38) and (39) is:

$$\delta \mathscr{L}^b_{int} = \int_L \delta \mathbf{v}_b^T \widetilde{\mathbf{K}}_b \mathbf{v}_b dx \tag{41}$$

where $\mathbf{v}_b \in \mathbb{R}^{4(n_b+1)}$ is organised as follows:

$$\mathbf{v}_b^T = \Big\{ u_0^b \quad u_1^b \quad \cdots \quad u_{n_b}^b \quad u_{0,x}^b \quad u_{1,x}^b \quad \cdots \quad u_{n_b,x}^b \quad w_0^b \quad w_1^b \quad \cdots \quad w_{n_b}^b \quad w_{0,x}^b \quad w_{1,x}^b \quad \cdots \quad w_{n_b,x}^b \Big\} \tag{42}$$

and $\widetilde{\mathbf{K}}_b \in \mathbb{R}^{4(n_b+1)\times 4(n_b+1)}$ is the bottom layer stiffness matrix.

3.2.2. Displacement continuity constraints between core and bottom layers

The congruency of the displacement field at core and bottom layers' interface Γ is enforced by means of the Lagrange multiplier $\boldsymbol{\mu}$ through the term $\delta\mathscr{C}$ in Eq. (18). This latter is obtained by applying the virtual variation operator to Eq. (10):

$$\begin{aligned}\delta\mathscr{C}(\boldsymbol{\mu},\mathbf{u}) &= \mathscr{C}(\delta\boldsymbol{\mu},\mathbf{u}) + \mathscr{C}(\boldsymbol{\mu},\delta\mathbf{u}) \\ &= \int_\Gamma \left\{ \delta\mu_1 \left[u^c(x,h_b) - u^b(x,h_b) \right] + \delta\mu_2 \left[w^c(x,h_b) - w^b(x,h_b) \right] \right\} d\Gamma \\ &\quad + \int_\Gamma \left\{ \mu_1 \left[\delta u^c(x,h_b) - \delta u^b(x,h_b) \right] + \mu_2 \left[\delta w^c(x,h_b) - \delta w^b(x,h_b) \right] \right\} d\Gamma\end{aligned} \tag{43}$$

After replacing Eqs. (6), (9) and (43) reads:

$$\begin{aligned}\frac{\delta\mathscr{C}(\boldsymbol{\mu},\mathbf{u})}{b} &= \int_L \delta\mu_1 \left[u_0^f + \frac{h_f}{2} w_{0,x}^f + \left(\widetilde{F}_j - \overline{F}_j \right) u_j^c - \widetilde{F}_\sigma u_\sigma^b \right] dx \\ &\quad + \int_L \delta\mu_2 \left[w_0^f + \left(\widetilde{F}_j - \overline{F}_j \right) w_j^c - \widetilde{F}_\sigma w_\sigma^b \right] dx \\ &\quad + \int_L \mu_1 \left[\delta u_0^f + \frac{h_f}{2} \delta w_{0,x}^f + \left(\widetilde{F}_j - \overline{F}_j \right) \delta u_j^c - \widetilde{F}_\sigma \delta u_\sigma^b \right] dx \\ &\quad + \int_L \mu_2 \left[\delta w_0^f + \left(\widetilde{F}_j - \overline{F}_j \right) \delta w_j^c - \widetilde{F}_\sigma \delta w_\sigma^b \right] dx\end{aligned} \tag{44}$$

with $\widetilde{F}_r = h_b^r$. Eq. (44) can be written in a matrix compact form:

$$\delta\mathscr{C}(\boldsymbol{\mu},\mathbf{u}) = \int_L \delta\mathbf{v}_\mathscr{C}^T \widetilde{\mathbf{K}}_\mathscr{C} \mathbf{v}_\mathscr{C} dx \tag{45}$$

upon introduction of the vector $\mathbf{v}_\mathscr{C} \in \mathbb{R}^{4(n_c+n_b)+9}$:

$$\mathbf{v}_\mathscr{C}^T = \left\{ \mathbf{v}_c^T \mid \mathbf{v}_b^T \mid \boldsymbol{\mu}^T \right\} \tag{46}$$

3.2.3. Weak form of the governing equations

In order to obtain the weak form of the governing equations for the whole thin film/substrate system, the vector $\mathbf{v} \in \mathbb{R}^{4(n_c+n_b)+11}$ containing all the unknown functions and their derivatives should be defined:

$$\begin{aligned}\mathbf{v}^T = \Big\{ & u_0^f \; u_{0,x}^f \; w_0^f \; w_{0,x}^f \; w_{0,xx}^f \; u_1^c \; \cdots \; u_{n_c}^c \; u_{1,x}^c \; \cdots \; u_{n_c,x}^c \; w_1^c \; \cdots \\ & w_{n_c}^c \; w_{1,x}^c \; \cdots \; w_{n_c,x}^c \; u_0^b \; u_1^b \; \cdots \; u_{n_b}^b \; u_{0,x}^b \; u_{1,x}^b \; \cdots \; u_{n_b,x}^b \; w_0^b \; w_1^b \; \cdots \\ & w_{n_b}^b \; w_{0,x}^b \; w_{1,x}^b \; \cdots \; w_{n_b,x}^b \; \mu_1 \; \mu_2 \Big\}\end{aligned} \tag{47}$$

Furthermore, the dimension of the unknown vectors in Eqs. (24, 36, 42) and (46) should be expanded to be coherent with the global approximation space:

$$\begin{aligned}\mathbf{v}_f &= \mathbf{R}_f \mathbf{v} : \mathbf{R}_f \in \mathbb{R}^{3\times 4(n_c+n_b)+11} \\ \mathbf{v}_c &= \mathbf{R}_c \mathbf{v} : \mathbf{R}_c \in \mathbb{R}^{4n_c+3\times 4(n_c+n_b)+11} \\ \mathbf{v}_b &= \mathbf{R}_b \mathbf{v} : \mathbf{R}_b \in \mathbb{R}^{4(n_b+1)\times 4(n_c+n_b)+11} \\ \mathbf{v}_\mathscr{C} &= \mathbf{R}_\mathscr{C} \mathbf{v} : \mathbf{R}_\mathscr{C} \in \mathbb{R}^{4(n_c+n_b)+9\times 4(n_c+n_b)+11}\end{aligned} \tag{48}$$

where $\mathbf{R}_f, \mathbf{R}_c, \mathbf{R}_b$ and $\mathbf{R}_\mathscr{C}$ are approximation spaces expansion matrices. The total internal virtual work is finally expressed as:

$$\begin{aligned}\delta\mathscr{L}_{int} &= \int_L \delta\mathbf{v}^T \left[\mathbf{R}_f^T \left(\mathbf{H}^T + \mathbf{A}^{fT} \right) \mathbf{S}^f + \left(\mathbf{R}_c^T \widetilde{\mathbf{K}}_c \mathbf{R}_c + \mathbf{R}_b^T \widetilde{\mathbf{K}}_b \mathbf{R}_b + \mathbf{R}_\mathscr{C}^T \widetilde{\mathbf{K}}_\mathscr{C} \mathbf{R}_\mathscr{C} \right) \mathbf{v} \right] dx \\ &= \int_L \delta\mathbf{v}^T \left[\mathbf{R}_f^T \left(\mathbf{H}^T + \mathbf{A}^{fT} \right) \mathbf{S}^f + \widetilde{\mathbf{K}}_s \mathbf{v} \right] dx\end{aligned} \tag{49}$$

with:

$$\mathbf{S}^f = \mathbf{D}^f \left(\mathbf{H} + \frac{1}{2} \mathbf{A}^f \right) \mathbf{R}_f \mathbf{v} \tag{50}$$

and:

$$\widetilde{\mathbf{K}}_s = \mathbf{R}_c^T \widetilde{\mathbf{K}}_c \mathbf{R}_c + \mathbf{R}_b^T \widetilde{\mathbf{K}}_b \mathbf{R}_b + \mathbf{R}_\mathscr{C}^T \widetilde{\mathbf{K}}_\mathscr{C} \mathbf{R}_\mathscr{C} \tag{51}$$

This latter term has been introduced for the sake of brevity. A generalised load vector $\lambda\mathbf{f}$ per unit length and width is considered for determining the external virtual work:

$$\delta\mathscr{L}_{ext} = \lambda b \int_L \delta\mathbf{v}^T \mathbf{f} dx \tag{52}$$

3.3. Finite element discretisation

Eqs. (49) and (52) are discretised using the finite element method. Two-node one-dimensional elements are considered. The axial displacement components and the Lagrange multiplier are approximated by means of Lagrange linear shape functions $L_l(\xi)$, whereas Hermite quadratic polynomials $H_l(\xi)$ are used for the transverse displacement components and its derivatives, see Bathe [29]. Subscript l ranges in $[1,2]$ and $\xi \in [-1,+1]$ is the element natural dimensionless coordinate. The generic shape function is addressed by $N_l(\xi)$ such that the approximation of the generic component v_k of $\mathbf{v}$ can be expressed as:

$$v_k(x) = N_l(\xi(x)) q_l^k \quad l \in [1,2] \subset \mathbb{N} \tag{53}$$

q_l^k is a generic component of the vector of degrees of freedoms (DOFs) $\mathbf{q}_l \in \mathbb{R}^{3(n_c+n_b)+8}$ for node l:

$$\begin{aligned}\mathbf{q}_l^T = \Big\{ & q_l^{u_0^f} \; q_l^{w_0^f} \; q_l^{w_{0l,x}^f} \; q_l^{u_1^c} \; \cdots \; q_l^{u_{n_c}^c} \; q_l^{w_1^c} \; \cdots \; q_l^{w_{n_c}^c} \; q_l^{w_{1,x}^c} \; \cdots \\ & q_l^{w_{n_c,x}^c} \; q_l^{u_0^b} \; q_l^{u_1^b} \; \cdots \; q_l^{u_{n_b}^b} \; q_l^{w_0^b} \; q_l^{w_1^b} \; \cdots \; q_l^{w_{n_b}^b} \; q_l^{w_{0,x}^b} \; q_l^{w_{1,x}^b} \; \cdots \; q_l^{w_{n_b,x}^b} \; q_l^{\mu_1} \; q_l^{\mu_2} \Big\}\end{aligned} \tag{54}$$

Element's vector of DOFs $\mathbf{q} \in \mathbb{R}^{2[3(n_c+n_b)+8]}$ is:

$$\mathbf{q}^T = \left\{ \mathbf{q}_1^T \mid \mathbf{q}_2^T \right\} \tag{55}$$

Eqs. (53) can be written in the following compact matrix form:

$$\mathbf{v} = \mathbf{G}\mathbf{q} \tag{56}$$

where $\mathbf{G} \in \mathbb{R}^{[4(n_c+n_b)+11]\times 2[3(n_c+n_b)+8]}$ is a matrix containing the shape functions and their derivatives versus the axial coordinate. Finally, the principle of virtual displacement at element level is:

$$\begin{aligned}&\int_{L_e} \mathbf{G}^T \left\{ \left[\mathbf{R}_f^T \left(\mathbf{H}^T + \mathbf{A}^{fT} \right) \mathbf{D}^f \left(\mathbf{H} + \frac{1}{2} \mathbf{A}^f \right) \mathbf{R}_f + \widetilde{\mathbf{K}}_s \right] \mathbf{G} \right\} dx \mathbf{q} \\ &\quad = \lambda b \int_{L_e} \mathbf{G}^T \mathbf{f} dx\end{aligned} \tag{57}$$

where L_e is the length of the element.

The governing equation for the entire structure is obtained upon assembling the element matrices for each element using classical finite element procedures. This results in a global non-linear algebraic problem:

$$\mathbf{R}(\boldsymbol{\Theta};\lambda) = 0 \tag{58}$$

where $\boldsymbol{\Theta}$ is the global unknown vector whose dimension is N. The problem is solved by means of the asymptotic numerical method. Solution details are provided in the next section.

4. Solution of the non-linear problem

Assuming that a solution of Eq. (58) at point j is known, the solution $(\boldsymbol{\Theta};\lambda)^{j+1}$ at point $j+1$ is obtained from this latter following a perturbation technique. An approached solution path at step $j+1$ is represented by a n-order Taylor series expansion of $\boldsymbol{\Theta}$ and λ:

$$\begin{aligned}\boldsymbol{\Theta}^{j+1} &= \boldsymbol{\Theta}^{j} + a^{p}\boldsymbol{\Theta}_{p} \\ \lambda^{j+1} &= \lambda^{j} + a^{p}\lambda_{p}\end{aligned} \quad p \in [1,n] \tag{59}$$

where $a \in \mathbb{R}$ is a solution path parameter for the non-linear problem and $n(N+1)$ unknowns are present in the approximation in Eq. (59). By replacing Eq. (59) within the non-linear problem, Eq. (58) reads:

$$\mathbf{R}\left(\boldsymbol{\Theta}^{j} + a^{p}\boldsymbol{\Theta}_{p}; \lambda^{j} + a^{p}\lambda_{p}\right) = 0 \tag{60}$$

Its n-order Taylor series expansion about the point $(\boldsymbol{\Theta};\lambda)^{j}$ is, then:

$$\begin{aligned}&\mathbf{R}\left(\boldsymbol{\Theta}^{j};\lambda^{j}\right) + \left.\frac{\partial \mathbf{R}}{\partial \boldsymbol{\Theta}}\right|_{j} a^{p}\boldsymbol{\Theta}_{p} + \left.\frac{\partial \mathbf{R}}{\partial \lambda}\right|_{j} a^{p}\lambda_{p} + \frac{1}{2}\left[\left.\frac{\partial^{2}\mathbf{R}}{\partial \boldsymbol{\Theta}^{2}}\right|_{j} a^{p}\boldsymbol{\Theta}_{p}a^{s}\boldsymbol{\Theta}_{s} + \left.\frac{\partial^{2}\mathbf{R}}{\partial \lambda^{2}}\right|_{j} a^{p}\lambda_{p}a^{s}\lambda_{s}\right. \\ &\left. + \left.\frac{\partial^{2}\mathbf{R}}{\partial \boldsymbol{\Theta}\partial \lambda}\right|_{j} a^{p}\boldsymbol{\Theta}_{p}a^{s}\lambda_{s}\right] + \frac{1}{3!}\left[\left.\frac{\partial^{3}\mathbf{R}}{\partial \boldsymbol{\Theta}^{3}}\right|_{j} a^{p}\boldsymbol{\Theta}_{p}a^{s}\boldsymbol{\Theta}_{s}a^{q}\boldsymbol{\Theta}_{q} + \left.\frac{\partial^{3}\mathbf{R}}{\partial \lambda^{3}}\right|_{j} a^{p}\lambda_{p}a^{s}\lambda_{s}a^{q}\lambda_{q}\right. \\ &\left. + \left.\frac{\partial^{3}\mathbf{R}}{\partial \boldsymbol{\Theta}^{2}\partial \lambda}\right|_{j} a^{p}\boldsymbol{\Theta}_{p}a^{s}\boldsymbol{\Theta}_{s}a^{q}\lambda_{q} + \left.\frac{\partial^{3}\mathbf{R}}{\partial \boldsymbol{\Theta}\partial \lambda^{2}}\right|_{j} a^{p}\boldsymbol{\Theta}_{p}a^{s}\lambda_{s}a^{q}\lambda_{q}\right] + \ldots = 0\end{aligned} \tag{61}$$

where $\mathbf{R}\left(\boldsymbol{\Theta}^{j};\lambda^{j}\right) = 0$ since $(\boldsymbol{\Theta};\lambda)^{j}$ belongs to the solution domain. Eq. (61) can be re-arranged in the following manner:

$$\begin{aligned}\mathbf{R}(\boldsymbol{\Theta};\lambda) = {} & a\left[\left.\frac{\partial \mathbf{R}}{\partial \boldsymbol{\Theta}}\right|_{j}\boldsymbol{\Theta}_{1} + \left.\frac{\partial \mathbf{R}}{\partial \lambda}\right|_{j}\lambda_{1}\right] \\ & + a^{2}\left\{\left.\frac{\partial \mathbf{R}}{\partial \boldsymbol{\Theta}}\right|_{j}\boldsymbol{\Theta}_{2} + \left.\frac{\partial \mathbf{R}}{\partial \lambda}\right|_{j}\lambda_{2} + \frac{1}{2}\left[\left.\frac{\partial^{2}\mathbf{R}}{\partial \boldsymbol{\Theta}^{2}}\right|_{j}\boldsymbol{\Theta}_{1}^{2} + \left.\frac{\partial^{2}\mathbf{R}}{\partial \lambda^{2}}\right|_{j}\lambda_{1}^{2} + \left.\frac{\partial^{2}\mathbf{R}}{\partial \boldsymbol{\Theta}\partial \lambda}\right|_{j}\boldsymbol{\Theta}_{1}\lambda_{1}\right]\right\} \\ & + a^{3}\left[\left.\frac{\partial \mathbf{R}}{\partial \boldsymbol{\Theta}}\right|_{j}\boldsymbol{\Theta}_{3} + \left.\frac{\partial \mathbf{R}}{\partial \lambda}\right|_{j}\lambda_{3} - \mathscr{F}_{3}(\boldsymbol{\Theta}_{1},\boldsymbol{\Theta}_{2};\lambda_{1},\lambda_{2})\right] + \ldots \\ & + a^{n}\left[\left.\frac{\partial \mathbf{R}}{\partial \boldsymbol{\Theta}}\right|_{j}\boldsymbol{\Theta}_{n} + \left.\frac{\partial \mathbf{R}}{\partial \lambda}\right|_{j}\lambda_{n} - \mathscr{F}_{n}(\boldsymbol{\Theta}_{1},\boldsymbol{\Theta}_{2},\ldots,\boldsymbol{\Theta}_{n-1};\lambda_{1},\lambda_{2},\ldots,\lambda_{n-1}) = 0\right]\end{aligned} \tag{62}$$

where, for a given order p of a, $\mathscr{F}_{p}$ is a function of the unknowns $\boldsymbol{\Theta}_{k}$ and λ_{k} with $k \in [1, p-1]$. Eq. (62) must be valid for a generic value of a, therefore, the following linear system of N equations in $N+1$ unknowns:

$$\left.\frac{\partial \mathbf{R}}{\partial \boldsymbol{\Theta}}\right|_{j}\boldsymbol{\Theta}_{p} + \left.\frac{\partial \mathbf{R}}{\partial \lambda}\right|_{j}\lambda_{p} = \mathscr{F}_{p}\left(\boldsymbol{\Theta}_{1},\boldsymbol{\Theta}_{2},\ldots,\boldsymbol{\Theta}_{p-1};\lambda_{1},\lambda_{2},\ldots,\lambda_{p-1}\right) \tag{63}$$

is obtained from each term a^{p} and n linear systems are obtained in total. $\mathscr{F}_{p}$ is known once the linear system derived form the orders lower than the p-th one have been solved. The problem in Eq. (63) is not well posed and a complementary condition for each expansion term p should be provided. This complementary condition is obtained from the definition of the path parameter a as a pseudo-arc-length by projecting the solution increment $(\boldsymbol{\Theta};\lambda)^{j+1} = \left(\boldsymbol{\Theta} - \boldsymbol{\Theta}^{j};\lambda - \lambda^{j}\right)$ over the tangent direction $(\boldsymbol{\Theta}_{1};\lambda_{1})$:

$$a = \left(\boldsymbol{\Theta} - \boldsymbol{\Theta}^{j}\right)^{T}\boldsymbol{\Theta}_{1} + \left(\lambda - \lambda^{j}\right)\lambda_{1} \tag{64}$$

The following equations are, then, obtained by replacing Eq. (59) within Eq. (64):

$$\begin{aligned}&\|\boldsymbol{\Theta}_{1}\|^{2} + \lambda_{1}^{2} = 1 \qquad p = 1 \\ &\boldsymbol{\Theta}_{p}^{T}\boldsymbol{\Theta}_{1} + \lambda_{p}\lambda_{1} = 0 \quad p \neq 1\end{aligned} \tag{65}$$

being $\|\square\|$ the Euclidean norm. The problem composed by Eqs. (63) and (65) is well posed since it comprises $n(N+1)$ unknowns as well as equations. At each step j, the matrix $\left.\frac{\partial \mathbf{R}}{\partial \boldsymbol{\Theta}}\right|_{j}$ is the same for each expansion term p. A relevant amount of calculation time is, therefore, saved since only one stiffness matrix has to be factored. Once the values $\boldsymbol{\Theta}_{p}$ and λ_{p} have been all computed, the path solution at step $j+1$ is obtained by Eq. (59). Finally, as reported in Cochelin et al. [24], the following relation between the path parameter a and the expansion order n holds:

$$a = \left(\epsilon\frac{\|\boldsymbol{\Theta}_{1}\|}{\|\boldsymbol{\Theta}_{n}\|}\right)^{\frac{1}{n-1}} \tag{66}$$

where ϵ is tolerance parameter (for a fixed n, the smaller ϵ, the shorter the solution step length).

5. Numerical results

A film-substrate system under compressive forces as illustrated in Fig. 2 is considered. The bottommost surface of the substrate ($z/h = 0$) is clamped. This kinematic boundary condition is obtained straightforwardly by imposing the nodal DOFs corresponding to u_{0}^{b}, w_{0}^{b} and $w_{0,x}^{b}$ equal to zero. The vertical displacement w is equal to zero at $x/L = 0$ and 1. Two concentrated forces of equal modulus F and opposite verse are applied along the axial direction at film through-the-thickness mid point. Table 1 presents the material properties and the geometric parameters. Young's moduli ratio E_{s}/E_{f} is as low as 10^{-6} and as high as 10^{-3}. The thickness ratio h_{s}/h_{f} ranges between 6 and $6\cdot 10^{3}$. This first case is addressed as "problem I". The obtained results are assessed towards numerical results obtained by a two-dimensional non-linear elasticity solution within the finite element code ABAQUS. The film is meshed using 3-node beam elements, whereas 8-node quadrilateral elements are used for the substrate. Unless differently stated, a 100×50 mesh is used. The total DOFs of this numerical solution are about $3.1\cdot 10^{4}$. Table 2 presents the critical load parameter λ_{c} and the corresponding half-wave number $n_{w}^{\lambda_{c}}$. Results have been computed via a $n_{c} = 5$ and $n_{b} = 3$ model. This kinematic model represents, for the considered cases, a good compromise between accuracy and computational costs (the effect of different expansion orders is later investigated). The film-substrate system is discretised along the axis into 120 elements. The DOFs of the proposed solution are equal to about $3.9\cdot 10^{3}$ (an order of magnitude lower than the reference two-dimensional solution). Results show that the proposed elements yield very good results. Some considerations on the obtained results can be drawn. The assumption of Euler–Bernulli kinematics for the thin film has been proved to be correct, resulting in accurate results and a limited number of degrees of freedom. As a comparison, the difference in the degrees of freedom number between the proposed approach and a model where a generic n_{f} order theory based upon Mac Laurin's polynomials is used also in the film is equal to $2n_{f}-1$. This number can be straightforwardly obtained noticing that the two approaches

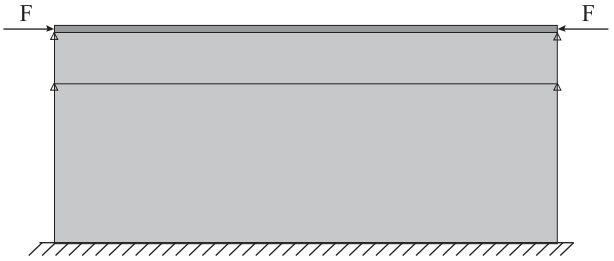

Fig. 2. Film-substrate load and boundary conditions.

Table 1
Problem I material and geometric parameters.

E_{f} (10^{4} MPa)	E_{s}/E_{f}	μ_{s}	L (10^{-1} m)	b (m)	h_{f}/L	h_{s}/h_{f}
6.9	$10^{-3}-10^{-6}$	0.3	5.0	1.0	1/600	$6-6\cdot 10^{3}$

Table 2
Half-wave number $n_w^{\lambda_c}$ and critical load parameter λ_c, problem I. One-dimensional solution via a $n_c = 5$ and $n_b = 3$ model with 120 axial elements.

h_s/h_f	6			$6 \cdot 10$			$6 \cdot 10^2$			$6 \cdot 10^3$		
	$n_w^{\lambda_c}$	$10^{-4}\lambda_c$		$n_w^{\lambda_c}$	$10^{-3}\lambda_c$		$n_w^{\lambda_c}$	$10^{-3}\lambda_c$		$n_w^{\lambda_c}$	$10^{-3}\lambda_c$	
E_s/E_f		1D	2D		1D	2D		1D	2D		1D	2D
10^{-3}	39	56.7	57.0	29	360	367	29	361	360	29	361	360
10^{-4}	23	16.6	16.6	13	75.0	75.3	13	74.3	74.3	13	74.5	74.3
10^{-5}	13	5.05	5.05	7	17.5	17.5	6	15.9	15.9	6	15.9	15.9
10^{-6}	7	1.60	1.60	5	5.21	5.22	3	3.38	3.38	3	3.38	3.38

would differ only in the kinematic model of the film. The instability in the film/substrate is very similar to that in an elastic beam resting on a non-linear Winkler foundation, where the following formulas holds, see Damil and Potier–Ferry [30]:

$$\lambda_c = 2\sqrt{E_f I_f c_s} \quad n_w^{\lambda_c} = \sqrt[4]{\frac{c_s}{E_f I_f}} \tag{67}$$

being the critical load parameter the global minimum point for the curve buckling load versus half-wave number ($\lambda_c = \min \lambda(n_w)$). $E_f I_f$ and c_s are the stiffness of the thin film and the substrate, respectively. For a fixed E_f, h_f and h_s, the stiffness of the film is constant and that of the substrate depends only upon the material parameter E_s. Under these circumstances:

$$\lambda_c \propto \sqrt{c_s(E_s)} \quad n_w^{\lambda_c} \propto \sqrt[4]{c_s(E_s)} \tag{68}$$

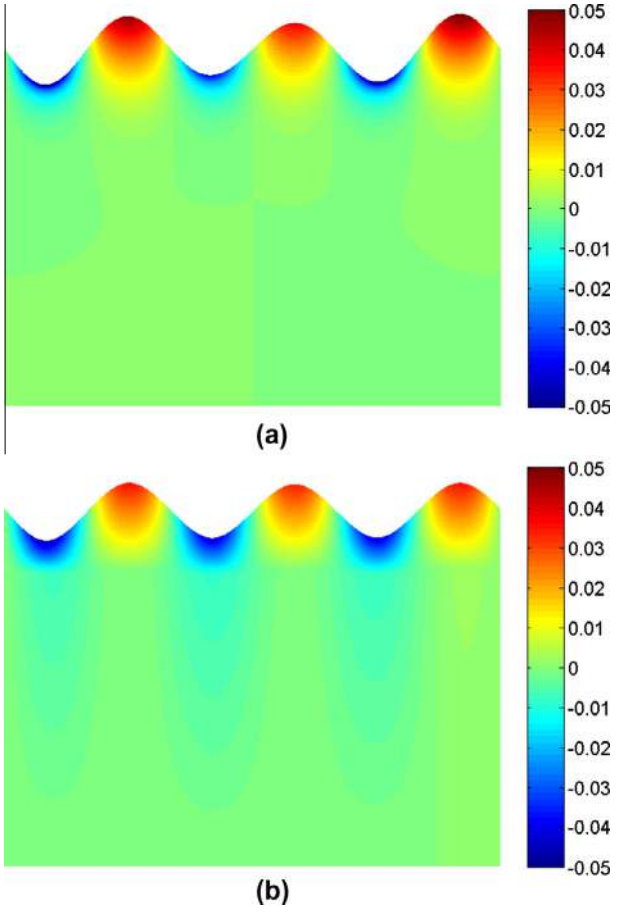

Fig. 3. Transverse displacement $10 \cdot w(\mathrm{m})$ colour map via (a) two-dimensional solution and (b) $n_c = 5$ and $n_b = 3$ one-dimensional model. Problem I, $E_s/E_f = 10^{-5}$ and $h_s/h_f = 6 \cdot 10^2$.

and this explain the reason why for each column of Table 2, $\lambda_c = O\left(c_s^{1/2}\right)$ and $n_w^{\lambda_c} = O\left(c_s^{1/4}\right)$ decrease as E_s/E_f is decreased. At the limit $E_s/E_f \to 0$, λ_c is expected to be equal to the Eulerian critical buckling load. Furthermore, for a fixed E_s/E_f ratio, λ_c and $n_w^{\lambda_c}$ become constant after a threshold value of h_s/h_f. This is due to the fact that only a limited part of the substrate in the neighbourhood of the thin film is involved by the instability phenomenon and the remaining part of the substrate remains unstrained. This is evident from Fig. 3 where the transverse displacement obtained by the 2D solution (60×30 mesh and $1.1 \cdot 10^4$ DOFs) and the proposed approach (30 elements and $1.0 \cdot 10^3$ DOFs) is plotted as a colour map for the case $E_s/E_f = 10^5$ and $h_s/h_f = 6 \cdot 10^2$.

Fig. 4 presents the variation of the transverse displacement at point $(x = L/4, z = h_s + h_f/2)$ versus the applied load per unit width F. The critical load computed via the 2D model is also presented. Results show a very good agreement.

5.1. Parametric investigation

The same loading and boundary conditions as shown in Fig. 2 are here considered, whereas the material properties and the geometrical data are presented in Table 3. This case is addressed as "problem II". The instability pattern for this second problem is first presented in Fig. 5. Results are computed through a $n_c = 5$ and $n_b = 3$ one-dimensional model with 110 elements along the axis. The same axial discretisation has been used for the ABAQUS solution. This is a limitation inherent to the solution of wrinkling problems by means of the finite element methods. The higher the half-wave number, the higher the number of elements to accu-

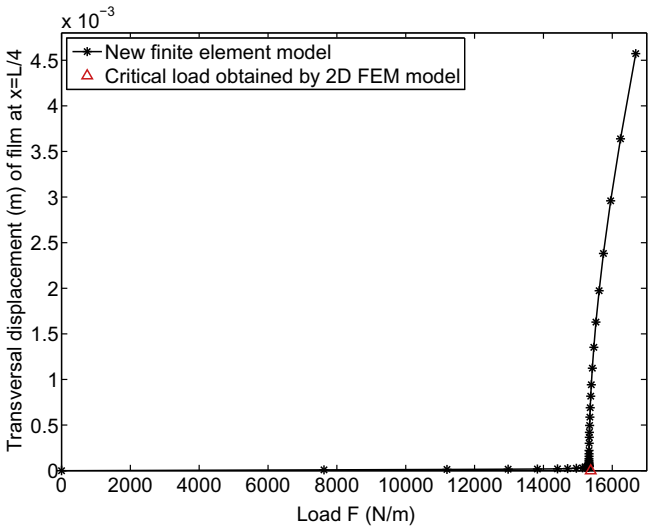

Fig. 4. Transverse displacement at $(x = L/4, z = h_s + h_f/2)$ versus the load per unit width F (bifurcation curve). Problem I, $E_s/E_f = 10^{-5}$ and $h_s/h_f = 6 \cdot 10^2$.

Table 3
Problem II material and geometric parameters.

E_f (10^5 MPa)	E_s/E_f	μ_s	L (10^{-3} m)	b (10^{-3} m)	h_f/L	h_s/h_f
1.8	10^{-5}	0.3	1.0	1.0	10^{-3}	10^3

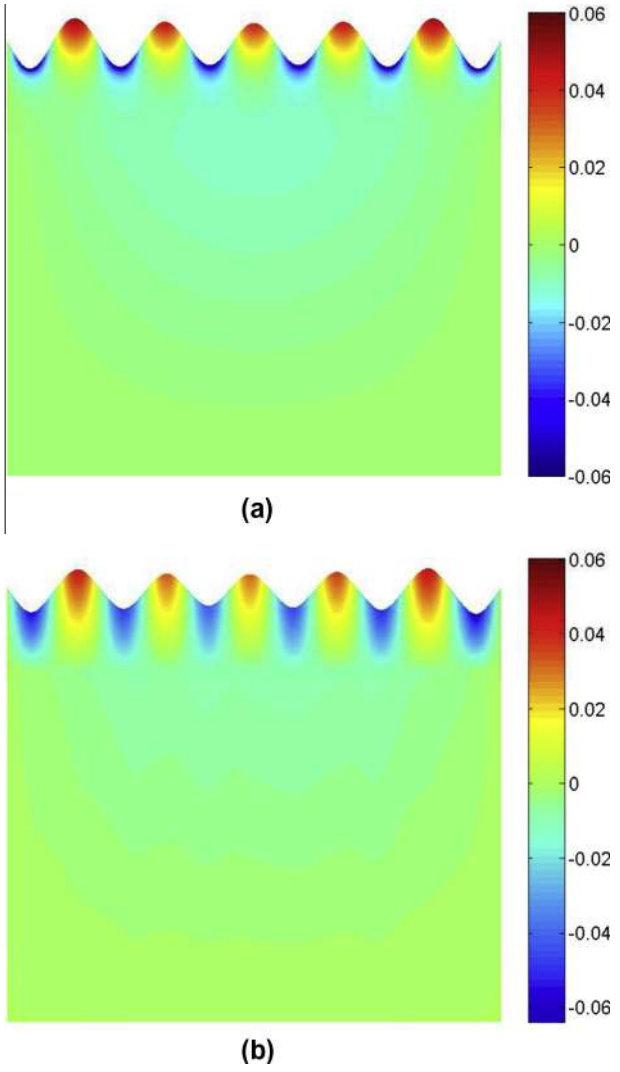

Fig. 5. Transverse displacement $10 \cdot w$ (10^{-3} m) colour map via (a) two-dimensional solution and (b) $n_c = 5$ and $n_b = 3$ one-dimensional model. Problem II, $E_s/E_f = 10^{-5}$ and $h_s/h_f = 6 \cdot 10^2$.

rately model the problem. As a future perspective, a reduced-order technique (for instance, using a Fourier-related analysis as in Liu et al. [26]) will be developed in the framework of the present finite elements family. The bifurcation load obtained by the two-dimensional solution is also presented and a very good agreement is observed.

In order to better outline the idea behind the present work (that is, ideally splitting the substrate in two different parts) as well as to stress the importance of the right choice for the value of h_c out, the through-the-thickness variation of the transverse displacement computed by the two-dimensional model is presented in Fig. 6. The size of the boundary layer, where w decreases from $0.8 \cdot 10^{-3}$ m to almost zero is a small fraction of the whole substrate thickness h_s that, for the considered case, is as wide as twice the wrinkles wavelength $\ell_w = L/n_w^c$. Fig. 7 presents the transverse

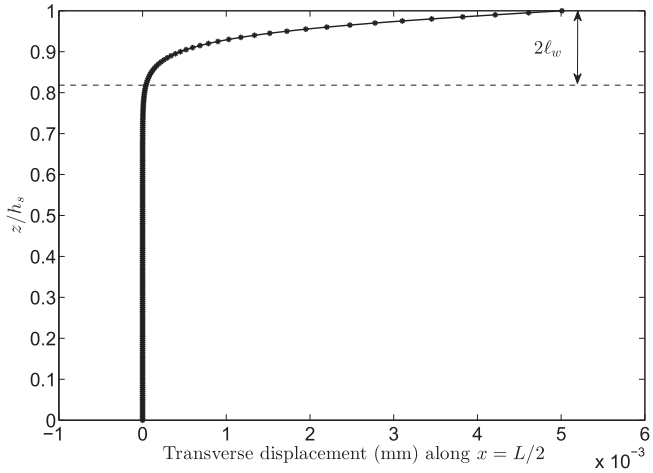

Fig. 6. Through-the-thickness variation of the transverse displacement at $x = L/2$, two-dimensional solution, problem II.

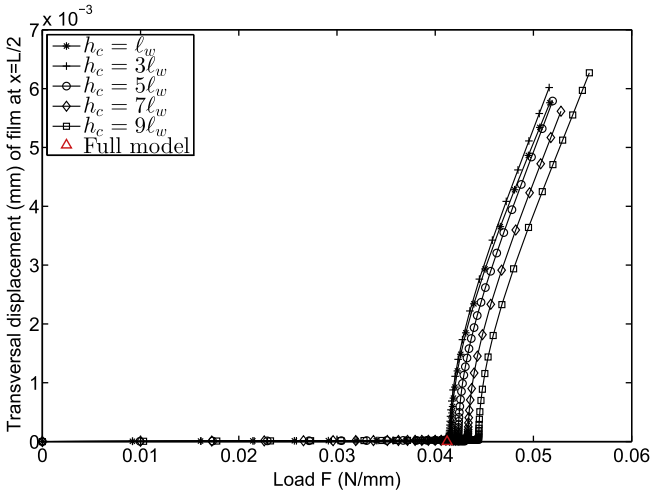

Fig. 7. Bifurcation curves at $(x = L/2, z = h_s + h_f/2)$ for different values of the core thickness (expressed as a multiple of the wrinkle wavelength ℓ_w), $n_c = 5$ and $n_b = 3$ one-dimensional model, problem II.

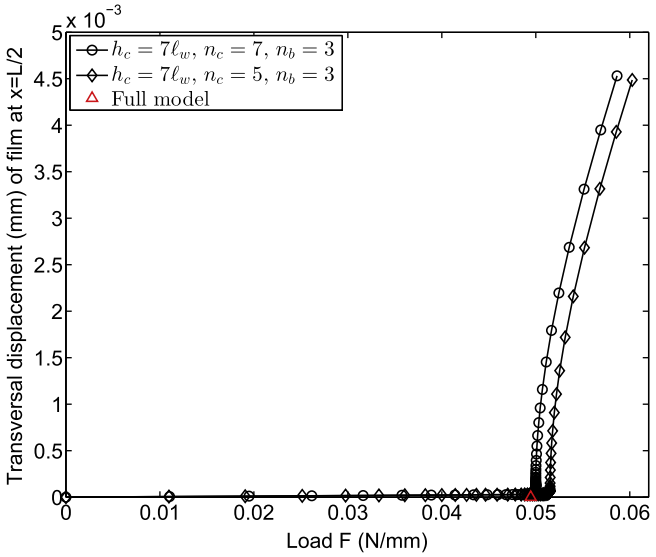

Fig. 8. Bifurcation curves at $(x = L/2, z = h_s + h_f/2)$ for $n_c = 5$ and 7 and $h_c = 7\ell_w$, problem II.

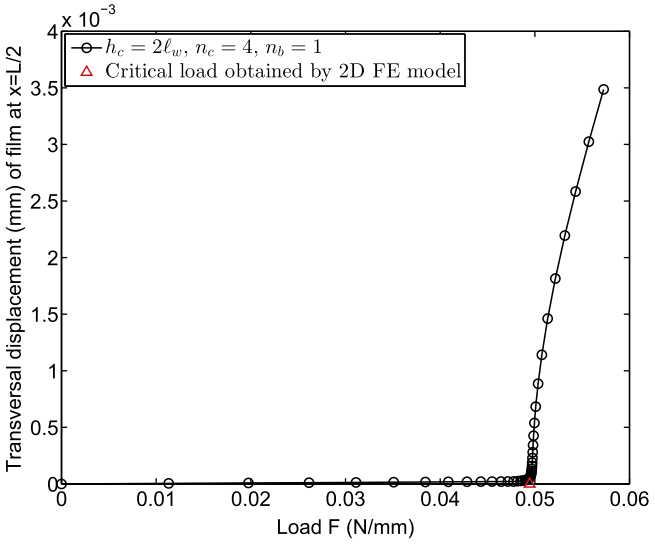

Fig. 9. Bifurcation curve at $(x = L/2, z = h_s + h_f/2)$ for $n_c = 4, n_b = 1$ and $h_c = 2\ell_w$, problem II.

displacement versus the applied load for various values of the core thickness. This latter is expressed as a multiple of the wrinkle wavelength in order to estimate the size of the "boundary layer" in terms of the mechanics of the problem. A correct choice of h_c is very important since, for a fixed expansion order n_c, its overestimation is counter-productive: the refined model is used in a fraction of the substrate that is too wide. Its effectiveness is, then, compromised. In a similar manner, an underestimated h_c yields poor results since the part of the solution presenting steep variations is approximated by the higher-order kinematic model only in part. Fig. 7 shows that $h_c = 3\ell_w$ represents a good estimation for the size of the "boundary layer". An increase in the expansion order n_c improves the results accuracy as presented in Fig. 8 where h_c has been appositely overestimated (it equals $7\ell_w$).

Finally, on the basis of Figs. 6 and 9 illustrates the bifurcation curve for $h_c = 2\ell_w$ with $n_c = 4$ and $n_b = 1$ and 55 elements along the x direction. This solution consists of about 10^3 DOFs. It demonstrates that the proposed approach can be effective for accurately yet effectively predicting the instability phenomena in thin film resting on substrates.

6. Conclusions

A family of one-dimensional variable kinematic elements for the study of local instabilities in thin films resting on compliant substrates has been addressed in this paper. Euler–Bernoulli's kinematics has been used for the thin film, whereas Carrera's Unified Formulation has been assumed for the substrate. This latter has been divided into two mathematical layers: a boundary layer where a higher-order model is used and a bottom layer with a low-order displacement field. The subdivision aimed at accurately and effectively model the mechanics of the considered structures that is characterised by a high through-the-thickness variation of the displacement field in a small area of the substrate in the neighbourhood of the thin film while the remaining part is almost unstrained. Results have been given in terms of critical wrinkling load and half-wave number. The full non-linear response in the form of bifurcation curves has been also presented. Parametric analyses have been carried out to investigate the effect of the material and geometrical parameters on the local instabilities. An estimation of the size of the mathematical core layer in terms of the wrinkles wavelength has been provided in order to better exploit the proposed approach. Several kinematics have been investigated with the intention to find the best compromise between accuracy and computational costs. Two-dimensional finite elements solutions have been also developed within ABAQUS for the sake of validation. By the numerical investigations, it has been shown that the present approach yields solutions very close to the full two-dimensional finite element model at a reduced computational cost (the degrees of freedom are an order of magnitude smaller). As a final remark, in the case of nearly periodic instability patterns, the proposed elements present the same drawbacks as full two-dimensional elements do: the control of the solution path is difficult when many equilibrium solutions and several secondary bifurcation points are present. A reduced-order technique (for instance, using a Fourier-related analysis as in Liu et al. [26]) will be developed in the framework of the present finite elements family as a future perspective.

Acknowledgements

This work has been supported by the National Natural Science Foundation of China (Grant No. 11372231) and the Science and Technology Agency of the Hubei Province of China (Grant No. 2011CDA047). The authors also gratefully acknowledge the financial support of the National Research Funds of Luxembourg through the project WRINKLE (Grant No. FNR/784868) and AMSINS (Grant No. INTER/MOBILITY/13/5660768).

References

[1] Bowden N, Brittain S, Evans AG, Hutchinson JW, Whitesides GM. Spontaneous formation of ordered structures in thin films of metals supported on an elastomeric polymer. Arch Comput Methods Eng 1998;393(6681):146–9.
[2] Volynskii AL, Bazhenov S, Lebedeva OV, Bakeev NF. Mechanical buckling instability of thin coatings deposited on soft polymer substrates. J Mater Sci 2000;35(3):547–54.
[3] Cao Y, Hutchinson JW. Wrinkling phenomena in neo-hookean film/substrate bilayers. J Appl Mech 2012;79(3):031019-1–9-9.
[4] Allen HG. Analysis & Design of Structural Sandwich Panels. Oxford, England: Pergamon Press; 1969.
[5] Niu K, Talreja R. Modeling of wrinkling in sandwich panels under compression. J Eng Mech 1999;125(8):875–83.
[6] Huang ZY, Hong W, Suo Z. Evolution of wrinkles in hard films on soft substrates. Phys Rev 2004;70(3):030601.
[7] Huang ZY, Hong W, Suo Z. Nonlinear analyses of wrinkles in a film bonded to a compliant substrate. J Mech Phys Solids 2005;53(9):2101–18.
[8] Audoly B, Boudaoud A. Buckling of a stiff film bound to a compliant substrate (Part I). Formulation, linear stability of cylindrical patterns, secondary bifurcations. J Mech Phys Solids 2008;56(7):2401–21.
[9] Audoly B, Boudaoud A. Buckling of a stiff film bound to a compliant substrate (Part II). A global scenario for the formation of herringbone pattern. J Mech Phys Solids 2008;56(7):2422–43.
[10] Audoly B, Boudaoud A. Buckling of a stiff film bound to a compliant substrate (Part III). Herringbone solutions at large buckling parameter. J Mech Phys Solids 2008;56(7):2444–58.
[11] Wang S, Song J, Kim D-H, Huang Y, Rogers JA. Local versus global buckling of thin films on elastomeric substrates. Appl Phys Lett 2008;93:023126-1–6-3.
[12] Zang J, Zhao X, Cao Y, Hutchinson JW. Localized ridge wrinkling of stiff films on compliant substrates. J Mech Phys Solids 2012;60(7):1265–79.
[13] Damil N, Potier-Ferry M. A generalized continuum approach to describe instability pattern formation by a multiple scale analysis. C R Méc 2006;334(11):674–8.
[14] Hu H, Damil N, Potier-Ferry M. A bridging technique to analyze the influence of boundary conditions on instability patterns. J Comput Phys 2011;230(10):3753–64.
[15] Xu F, Hu H, Potier-Ferry M, Belouettar S. Bridging techniques in a multi-scale modeling of pattern formation. Int J Solids Struct 2014;51(18):3119–34.
[16] Carrera E. Theories and finite elements for multilayered plates and shells: a unified compact formulation with numerical assessment and benchmarking. Arch Comput Methods Eng 2003;10(3):215–96.
[17] Carrera E, Giunta G. Hierarchical models for failure analysis of plates bent by distributed and localized transverse loadings. J Zhejiang Univ SCI A 2008;9(5):600 613.
[18] Carrera E, Giunta G. Exact, hierarchical solutions for localised loadings in isotropic, laminated and sandwich shells. J Pressure Vessel Technol 2009;131(4):041202.

[19] Carrera E, Giunta G. Refined beam theories based on a unified formulation. Int J Appl Mech 2010;2(1):117–43.
[20] Catapano A, Giunta G, Belouettar S, Carrera E. Static analysis of laminated beams via a unified formulation. Comput Struct 2011;94(1):75–83.
[21] He QZ, Hu H, Belouettar S, Guinta G, Yu K, Liu Y, et al. Multi-scale modelling of sandwich structures using hierarchical kinematics. Compos Struct 2011;93(9):2375–83.
[22] Damil N, Potier-Ferry M. A new method to compute perturbed bifurcation: Application to the buckling of imperfect elastic structures. Int J Eng Sci 1990;26:943–57.
[23] Cochelin B, Damil N, Potier-Ferry M. Asymptotic-numerical methods and padé approximants for nonlinear elastic structures. Int J Numer Methods Eng 1994;37:1187–213.
[24] Cochelin B, Damil N, Potier-Ferry M. Méthode Asymoptotique Numérique. Hermès-Lavoisier; 2007.
[25] Hu H, Belouettar S, Potier-Ferry M, Daya EM. Multi-scale modeling of sandwich structure using the Arlequin method, Part I: linear modelling. Finite Elem Anal Des 2009;45:37–51.
[26] Liu Y, Yu K, Hu H, Belouettar S, Potier-Ferry M, Damil N. A new Fourier-related double scale analysis for instability phenomena in sandwich structures. Int J Solids Struct 2012;49(22):3077–88.
[27] Carrera E, Brischetto S. Analysis of thickness locking in classical, refined and mixed multilayered plate theories. Compos Struct 2008;82(4):549–62.
[28] Giunta G, Biscani F, Belouettar S, Ferreira AJM, Carrera E. Free vibration analysis of composite beams via refined theories. Compos Part B 2013;44(1):540–52.
[29] Bathe KJ. Finite Element Procedure. Prentice Hall; 1996.
[30] Damil N, Potier-Ferry M. Influence of local wrinkling on membrane behaviour: a new approach by the technique of slowly variable fourier coefficients. J Mech Phys Solids 2010;58(8):1139–53.